Disruption of VGLUT1 in cholinergic medial habenula projections increases nicotine self-administration

Elizabeth A. Souter[1]; Yen-Chu Chen[2]; Vivien Zell[1]; Valeria Lallai[2]; Thomas Steinkellner[1]; William S. Conrad[1]; William Wisden[3]; Kenneth D. Harris[4]; Christie D. Fowler [2]; Thomas S. Hnasko[1,5]

[1]Department of Neurosciences, University of California, San Diego, La Jolla, CA 92093, USA
[2]Department of Neurobiology and Behavior sciences, University of California, Irvine, Irvine, CA 92697, USA
[3]Department of Life Sciences & UK Dementia Research Institute, Imperial College London, London SW7 2AZ, UK
[4]Institute of Neurology, University College London, Queen Square, London WC1N 3BG, UK
[5]Research Service VA San Diego Healthcare System, San Diego, CA 92161, USA
Correspondence and material requests should be addressed to T.S.H.
(thnasko@health.ucsd.edu; 9500 Gilman Drive, La Jolla CA 92093; 858 822 0672)

ABSTRACT

Cholinergic projections from the medial habenula (MHb) to the interpeduncular nucleus (IPN) have been studied for their complex contributions to nicotine addiction and have been implicated in nicotine reinforcement, aversion, and withdrawal. While it has been established that MHb cholinergic projections co-release glutamate, no direct evidence has demonstrated a role for this specific glutamate projection in nicotine consumption. In the present study, a novel floxed *Slc17a7* (VGLUT1) mouse was generated and used to create conditional knockout (cKO) mice that lack VGLUT1 in MHb cholinergic neurons. Histochemical approaches and optogenetics-assisted electrophysiology were used to validate the disruption of VGLUT1 from cholinergic MHb to IPN projections. The mice displayed no gross phenotypic abnormalities and exhibited normal exploratory and locomotor behavior in the open-field assay. However, the loss of VGLUT1-mediated glutamate co-release led to increased nicotine self-administration. These findings indicate that glutamate co-release from ventral MHb cholinergic neurons opposes nicotine consumption and provide additional support for targeting this synapse to develop potential treatments to nicotine addiction.

KEYWORDS

Nicotine, acetylcholine (ACh), glutamate, co-release, medial habenula (MHb), interpeduncular nucleus (IPN), vesicular glutamate transporter (VGLUT1)

INTRODUCTION

Despite decades of research demonstrating the negative consequences of smoking and emerging evidence on harmful effects of electronic cigarettes, the use of tobacco products persists. In the United States, nicotine use among adolescents has increased in recent years. For instance, in 2019, 23% of middle and high school students reported use of a nicotine-containing product in the past 30 days, up from 9% in 2014 [1,2]. As the main psychoactive and addictive compound, nicotine remains at the forefront of this continuing public health crisis [3-6].

Nicotine mediates its psychoactive effect by acting on nicotinic acetylcholine receptors (nAChRs) in the brain. Within the mesolimbic circuit, including ventral tegmental area dopaminergic projections to nucleus accumbens, activation of nAChRs contribute to the rewarding effect of nicotine [7-14]. Conversely, the excitatory projection from medial habenula (MHb) to interpeduncular nucleus (IPN) has been identified as a key substrate upon which nicotine actions contribute to nicotine aversion [15-24].

Both MHb and IPN express high levels of several nAChR subunits, which modulate excitability and neurotransmission within this projection [25-30]. Mice lacking α5-containing nAChRs self-administered significantly more nicotine at high (typically aversive) doses, an effect which was rescued by re-expression of α5 nAChR subunit to the MHb-IPN pathway, suggesting that α5-containing nAChRs here are necessary for nicotine aversion [19]. Additionally, overexpression of β4 nAChR subunit leads to enhanced MHb activity and a strong aversive response to nicotine, which can be abolished by disruption of the α5 nAChR subunit in MHb [21]. More recently, it has been shown that knockdown of the α3 nAChR subunit in either the MHb or IPN increases nicotine intake in rats [24]. These data together suggest that nAChRs containing the α5, α3, and β4 subunits mediate aversive signaling in the MHb-IPN. Further, IPN projections to laterodorsal tegmentum (LDTg) are also strongly modulated by nicotine, and inhibiting this projection is sufficient to block nicotine aversion [31]. Together, these findings establish the importance of MHb-IPN projections in modulating intake of nicotine and encoding its aversive properties.

MHb-IPN projections are topographically organized, with ventral MHb cholinergic projections targeting central IPN and Substance P projections from dorsal MHb targeting lateral IPN [32,33]. The cholinergic ventral MHb expresses nAChRs and has been particularly implicated in nicotine aversion [19,21,26,28-30,34]. However, these neurons also express vesicular glutamate transporters (VGLUT) and can thus co-release both ACh and glutamate [20,35,36], raising the question of what the glutamate signal from MHb may contribute to nicotine intake. To address this question, we made a new conditional VGLUT1 mouse line and used it to generate conditional knock-out (cKO) mice that lack VGLUT1 in ventral MHb cholinergic neurons. We show that cKO mice have reduced glutamate transmission in MHb projections to IPN and that cKO mice display increased intravenous (IV) nicotine self-administration, consistent with a role for VGLUT1-mediated glutamate co-release at this circuit in opposing nicotine intake.

METHODS
Animals
Mice were used in accordance with the University of California, San Diego and the University of California, Irvine Institutional Animal Care and Use Committees. BAC transgenic Kiaa1107-Cre mice were obtained from GENSAT through the MMRRC (#034692-UCD). Kiaa-Cre mice were bred hemizygously with C57Bl/6J wildtype mice (Jackson Laboratory, 000664). VGLUT2-IRES-

90   Cre (*Slc17a6^Cre*) knock-in mice were ordered from Jackson Laboratory (#028863) and bred

91   homozygously or to C57BL6/J wildtype mice. All experiments were done in adult mice (aged

92   greater than 8wks) and in both males and females in approximately equal proportion.

93

VGLUT1 conditional allele

94

95   To generate VGLUT1-floxed mice (*Slc17a7*^flox), a targeting vector containing two loxP sites

96   flanking *Slc17a7* exons 4-7 and an FRT-flanked neomycin (Neo) resistance cassette was

97   electroporated into C57Bl/6-derived ES cells. Antibiotic (G418) resistant colonies were selected,

98   isolated, and amplified. The amplified clones were screened for homologous recombination at

99   the *Slc17a7* locus by PCR. Southern blot analysis was used to confirm both 3' and 5'

100   homologous recombination. Blastocysts were isolated from pregnant C57Bl/6J-Tyr^c-2J/J (albino

101   C57Bl/6) females, injected with one of six validated ES cell clones, and implanted into pseudo-

102   pregnant females. Chimeric males were bred to C57Bl/6 females with constitutive expression of

103   FLP recombinase to excise the Neo cassette in F1 offspring. F1 mice were crossed to C57Bl/6,

104   excision was confirmed by PCR and Southern blot, and these F2 mice were used to establish

105   the VGLUT1 floxed line (*Slc17a7^flox*). To generate conditional knock-out mice (*Kiaa^Cre;*

106   *Slc17a7^flox/flox*), Kiaa^Cre mice were bred to homozygous *Slc17a7^flox/flox* and resulting heterozygotes

107   (*Kiaa^Cre; Slc17a7^+/flox*) were then bred to homozygous *Slc17a7^flox/flox* mice. Mice were group

108   housed and maintained on a 12-hour light-dark cycle. Food and water were available *ad libitum*

109   except where noted.

110

Stereotactic surgery

111

112   For intracranial injections, mice (>4 weeks) were deeply anesthetized with isoflurane, placed in

113   a stereotaxic frame (Kopf), and bilaterally injected with AAV1-Ef1a-DIO-ChR2:mCherry (2 x

114   10^12, UNC Gene Therapy Center) into the MHb (LM = -1.15, AP = -1.58, DV = -2.42 and -2.00,

115   20° angle; right: LM = +0.95, AP = -1.58, DV = -2.42 and -2.00, 20° angle; mm relative to

116   *Bregma*). Two 150nL aliquots were given per hemisphere at 100nl/min using pulled glass

117   pipettes (Nanoject III, Drummond Scientific). Analgesic was given before and at least one day

118   after surgery (Carprofen, Zoetis, 5mg/kg s.c.). Mice were monitored daily for 5d after surgery

119   and allowed to recover for at least 21d before histological processing or 28d before

120   electrophysiological recordings.

121

Immunohistochemistry

122

123   Mice were deeply anesthetized with pentobarbital (200mg/kg s.c., VetOne) and transcardially

124   perfused for 2m with ice-cold phosphate buffered saline (PBS) then for 8 min with ice-cold 4%

125   paraformaldehyde (PFA) at a rate of 5-6ml/min. Brains were prepared as previously described

126   [37]. Primary antibodies used: DsRed (Rabbit, 1:2000, Clontech), VGLUT1 (Guinea Pig, 1:2000,

127   Synaptic Systems), VGLUT2 (Rabbit, 1:1000, Synaptic Systems), ChAT (Goat, 1:200, Millipore).

128   Secondary antibodies used (5ug/ml, Jackson ImmunoResearch): Alexa488 Donkey Anti-Goat

129   (705-545-147), Alexa 488 Donkey Anti-Guinea Pig (706-545-148), Alexa594 Donkey Anti-

130   Guinea Pig (706-585-148), Alexa 594 Donkey Anti-Rabbit (711-585-152), Alexa647 Donkey

131   Anti-Rabbit (711-605-152), Alexa647 Donkey Anti-Goat (705-605-147). Images were captured

132   using a Zeiss AxioObserver Z1 epifluorescence microscope (10x 0.45NA, 20x 0.75NA, or 63x

133   1.4NA objective) and Zen software. Densitometry was done with Fiji/ImageJ.

134

Fluorescent *in situ* hybridization

135

136   Mice were deeply anesthetized with pentobarbital before cervical dislocation. Brains were

137   prepared as previously described [37]. In situ hybridization was done using RNAscope Multiplex

138   Fluorescent Assay (Advanced Cell Diagnostics) according to manufacturer specification.

139 *Slc17a7* (503511), *ChAT* (408731-C2), and *Cre* (312281-C3) were coupled to Atto550,
140 Alexa647, and Alexa488, respectively and counterstained with DAPI. Images were captured
141 using a Zeiss AxioObserver Z1 epifluorescence microscope and processed with Zen software.
142

Open-Field Behavior

143
144 Mice were placed in an Open Field (30m) measuring 50x50 cm and their activity was recorded
145 and analyzed using AnyMaze software (San Diego Instruments). The field was cleaned with
146 70% ethanol between sessions. The field was segmented into a 5x5 grid, with the innermost 9
147 squares designated as the center.
148

Operant Behavior

149
150 Mice were mildly food-restricted to 85-90% of their free-feeding weight and were then trained to
151 lever press for food pellets (grain-based, 20 mg, 5TUM, TestDiet) on a two-lever operant task
152 across ascending fixed ratio (FR) schedules from 1 up to 5 lever presses, as previously
153 described [18]. At the start of the session, both levers were extended into the chamber and were
154 present throughout the 1-hr session. Responses on the active lever that met the FR criteria
155 resulted in the delivery of a food pellet, which was paired with a cue light for a 20-s time-out
156 period, resulting in the final reinforcement schedule of FR5TO20 for food training sessions 4-7.
157 Responses on the inactive lever were recorded but had no scheduled consequences. Testing
158 was conducted 6-7d/wk and behavioral responses were recorded with a MedPC interface (Med
159 Associates). Thereafter, subjects were anesthetized (isoflurane) and catheterized as previously
160 described [18,38]. The catheter tubing was passed subcutaneously from the animal's back to
161 the right jugular vein, a 1-cm length of catheter tip was inserted into the vein and tied with
162 surgical silk suture. Following surgery animals were allowed ≥48 hr to recover, and were then
163 provided 1-hr access to re-establish food responding under the FR5TO20 sec schedule until the
164 criteria of >30 pellets/session were again achieved. Mice were then transitioned to respond for
165 intravenous nicotine self-administration in lieu of food using the same FR5TO20 sec, 1-hr daily
166 sessions, 6-7d/wk, at the training dose of nicotine (0.03 mg/kg/infusion) for 8 d. For all doses,
167 nicotine (0.03 ml per infusion volume) was delivered through tubing into the intravenous
168 catheter by a Razel syringe pump (Med Associates). After achieving stable responding on the
169 0.03 mg/kg/infusion dose, mice were transitioned to the moderate dose of 0.1 mg/kg/infusion
170 nicotine for 5d. This dose results in a similar levels of drug intake as that found at higher doses
171 with behavioral titration via self-administration and was used to further establish baseline
172 responding in between access to each subsequent varying dose [18]. Next, the mice were
173 provided access to either the low 0.01 mg/kg/infusion or high 0.4 mg/kg/infusion dose for 5d,
174 and then re-established at baseline on 0.1 mg/kg/infusion for at least 2d, and thereafter given
175 access to the counterbalanced doses of either 0.01 or 0.4 mg/kg/infusion for an additional 5d.
176 Following re-establishing baseline for at least 2d, the mice were then provided access to
177 respond for saline vehicle. The mean of the final 3 days on each dose was calculated for each
178 subject. Catheters were flushed daily with physiological sterile saline solution (0.9% w/v)
179 containing heparin (100 units/mL). Catheter integrity was verified with the ultra-short-acting
180 barbiturate anesthetic Brevital (2%, methohexital sodium, Eli Lilly) at the end of the study.
181

Electrophysiological recordings

182
183 Recordings were performed on adult mice (7-12wks) as previously described [39]. mCherry-
184 labeled MHb terminals were visualized by epifluorescence and visually guided patch recordings
185 were made using infrared-differential interference contrast (IR-DIC) illumination (Axiocam MRm,
186 Examiner.A1, Zeiss). ChR2 was activated by flashing blue light (473 nm) through the light path
187 of the microscope using a light-emitting diode (UHP-LED460, Prizmatix) under computer

188 control. Neurons were held in voltage-clamp at -60 mV to record EPSCs in whole-cell
189 configuration and single-pulse photostimuli (5-ms or 1-s pulse width) were applied every 45 s
190 and 10 photo-evoked currents were averaged per neuron per condition. Stock solutions of
191 DNQX (10 mM in DMSO, Sigma) and mecamylamine hydrochloride (10 mM, Tocris) were
192 diluted 1,000-fold in ACSF and bath applied at 10 μM. Current sizes were calculated by using
193 peak amplitude from baseline.
194
195 **Statistics**
196 Data analysis was done using GraphPad Prism v9. Data were analyzed using t-test corrected
197 for multiple comparisons (Bonferroni-Sidak)(figures 2b, 2c, 2d), unpaired t-test (4c, 4d, 5f), RM
198 two-way ANOVA (Sidak post hoc)(5b, 5c, 5g), or RM three-way ANOVA (Sidak post hoc)(5d,
199 5e).
200
201 **RESULTS**
202 Generation of *Slc17a7* conditional knock-out from ventral MHb
203
204 To target cholinergic neurons of the MHb we used the Kiaa1107-Cre (*Kiaa^{Cre}*) transgenic line
205 that has been used previously to disrupt Choline acetyltransferase (ChAT) expression in MHb
206 [20]. The functional expression of *Cre recombinase* driven by *Kiaa1107* regulatory elements
207 was first validated by crossing to the Ai6 ZsGreen reporter [40] to generate *Kiaa^{Cre};*
208 *Rosa26^{ZsGreen}* mice (**figure 1a**). Robust ZsGreen fluorescence was seen in MHb, with densest
209 expression observed in ventral (basolateral and basomedial) MHb (**figure 1b**).
210
211 To disrupt VGLUT1 expression, we generated a novel mouse line carrying a VGLUT1
212 conditional allele (*Slc17a7^{flox}*) with exons 4-7 flanked by loxP sites (**figure 1c**). We next crossed
213 *Slc17a7^{flox}* mice to *Kiaa^{Cre}* to generate the VGLUT1 conditional knockout (cKO, *Kiaa^{Cre};*
214 *Slc17a7$^{flox/flox}$*). We then generated an RNAscope probe targeting exons 4-7 of *Slc17a7* and
215 used this together with probes against a cholinergic marker (*Chat*) and *Cre recombinase* on
216 sections from cKO and control (*Kiaa^{Cre}*) mice (**figure 1d-e**). The pattern of *Cre* expression was
217 identical for both genotypes and similar to the pattern observed in the ZsGreen reporter cross,
218 with robust expression in ventral MHb. *Chat* appeared unchanged across genotype and showed
219 high overlap with *Cre. C*onsistent with other reports, *Chat* expression was largely restricted to
220 ventral MHb [35,41-43].
221
222 Also consistent with other previous reports, *Slc17a7* (VGLUT1) was expressed throughout the
223 MHb in controls [35,44-46]. However, the cKO showed a markedly different pattern. In cKO
224 mice, *Slc17a7* (VGLUT1) was virtually eliminated from ventral MHb, but expression was intact in
225 dorsal (apical) MHb (**figure 1d-e**). These results indicate that our cKO successfully and
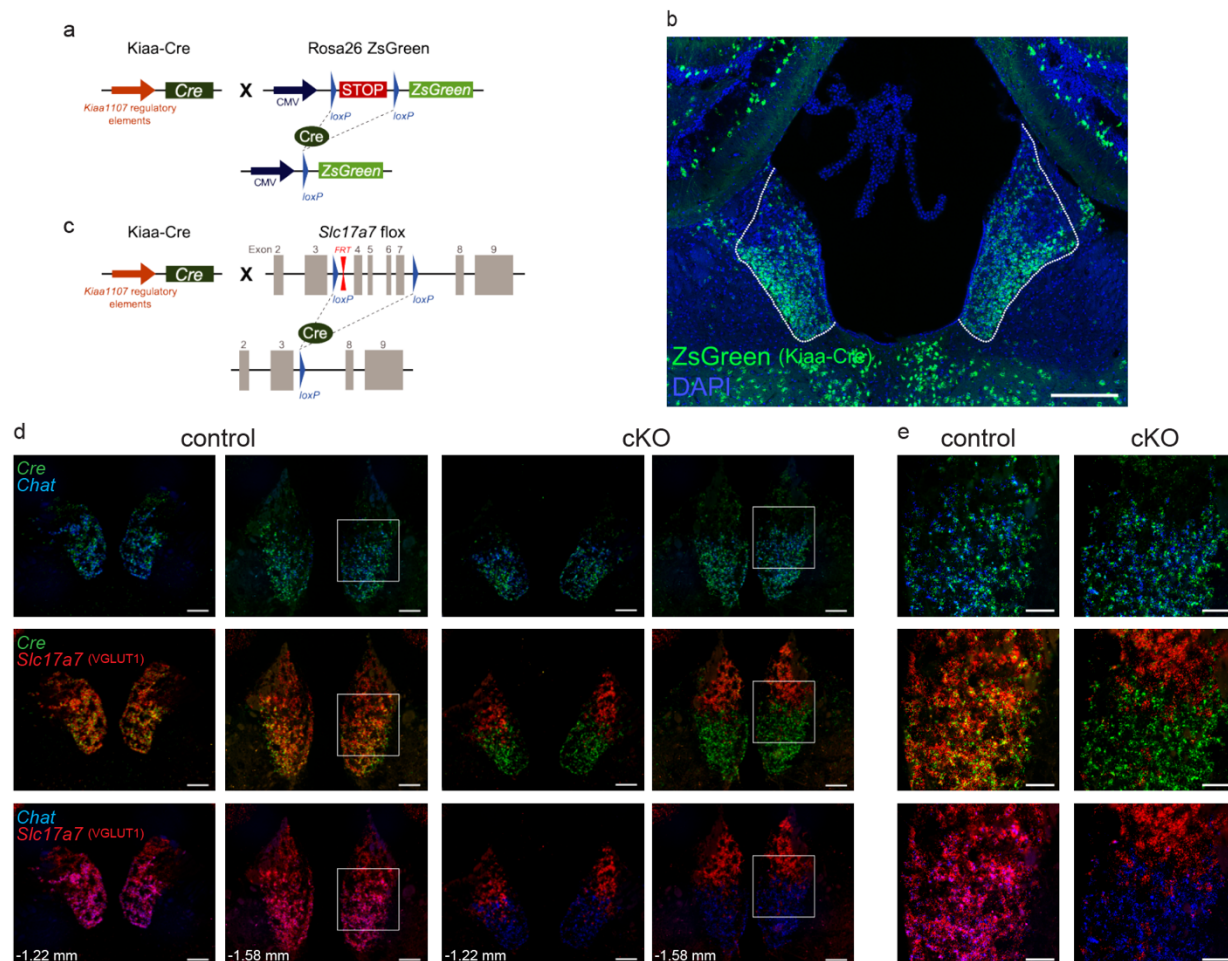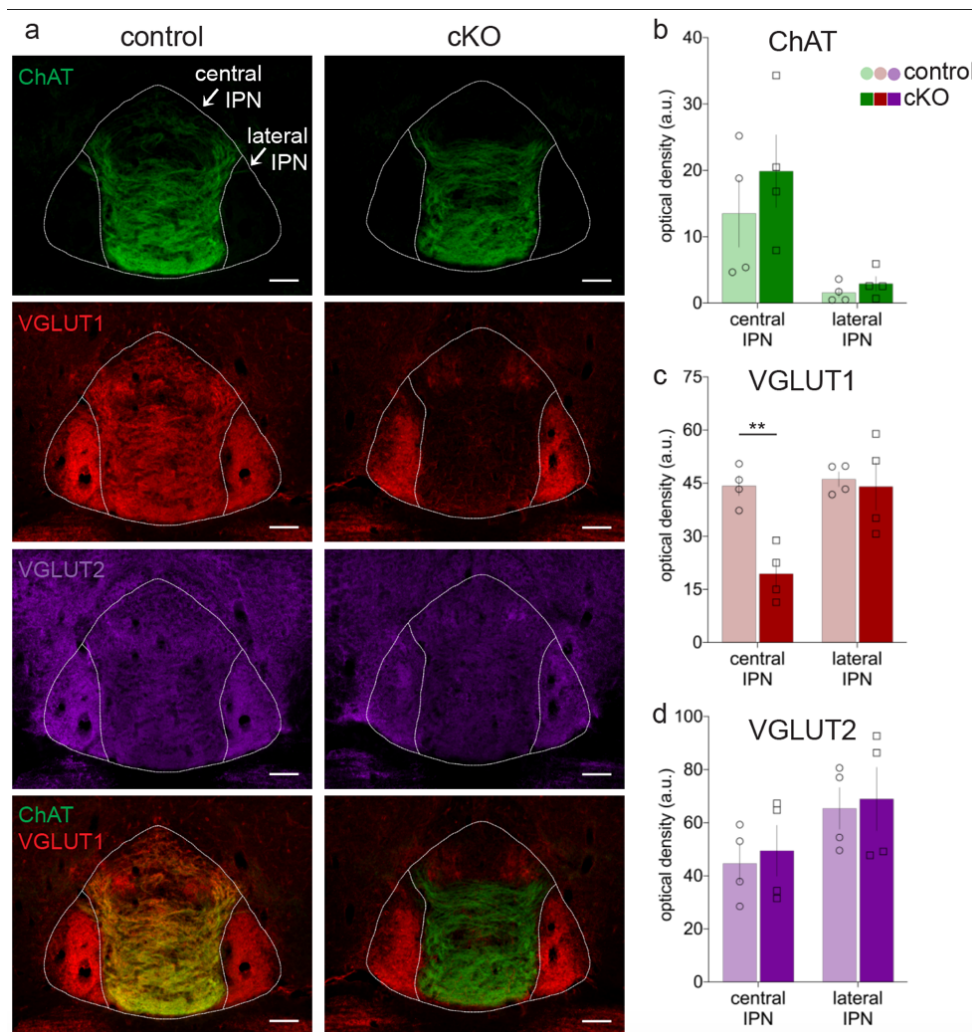226 selectively disrupted *Slc17a7* expression from Cre-expressing neurons in ventral MHb.
227
228

Figure 1. Conditional knock-out of *Slc17a7* (VGLUT1) from cholinergic neurons in MHb.
(a) Schematic of *Kiaa^Cre*; *Rosa26^ZSGreen* reporter mouse line with Cre expression driven by *Kiaa1107* regulatory elements and ZsGreen expression dependent on Cre recombination. **(b)** Native ZsGreen fluorescence counterstained with DAPI in MHb (outlined); scale 200 μm. **(c)** Schematic of Cre recombination of the floxed *Slc17a7* (VGLUT1) locus in the cKO (*Kiaa^Cre*; *Slc17a7^flox/flox*) mouse line. **(d)** Fluorescent *in situ* hybridization of *Cre*, *Chat*, and *Slc17a7* expression in MHb of control and cKO mice at two Bregma points; scale 100 μm. **(e)** Higher magnification images from white squares in (d); scale 50 μm.

We next used immunohistochemistry to examine the expression of pre-synaptic cholinergic and glutamatergic markers in the IPN, the major projection target of MHb (**figure 2a**). While the expression of ChAT was unaffected in the cKO (**figure 2b**), the pattern of VGLUT1-labeled fibers was markedly different depending on genotype and subregion. cKO mice had a significant reduction of VGLUT1 expression compared to controls in central IPN ($t(6)=5.2$, $p(adj)=0.004$), but no difference in VGLUT1 between genotypes was observed in lateral IPN ($t(6)=0.30$, $p(adj)=0.95$) (**figure 2c**). Together, these data are concordant with our RNAscope data and demonstrate the selective disruption of VGLUT1 from cholinergic MHb inputs that target the central region of the IPN, which includes the caudal, dorsomedial, intermediate, and rostral subnuclei.

249 We also examined VGLUT2-labeled fibers in the IPN to test whether the loss of VGLUT1 led to
250 changes in VGLUT2 expression. We detected no significant difference in VGLUT2 expression
251 between genotypes in either central IPN ($t(6)=0.41$, $p(adj)=0.91$) or lateral IPN ($t(6)=0.25$,
252 $p(adj)=0.96$) (**figure 2d**). These data argue against compensatory change in VGLUT2
253 expression following loss of VGLUT1 from cholinergic neurons in MHb.
254

255 **Figure 2: Loss of VGLUT1 in central IPN of cKO mice.**
256 (**a**) Immunohistochemistry for ChAT, VGLUT1, and VGLUT2 in the IPN of control ($Slc17a7^{flox}$)
257 and cKO mice ($Kiaa^{Cre}$; $Slc17a7^{flox/flox}$); bottom row shows ChAT and VGLUT1 merge; scale 100
258 μm. Densitometric quantification in central and lateral IPN of (**b**) ChAT, (**c**) VGLUT1, and (**d**)
259 VGLUT2 signals. Only VGLUT1 was significantly reduced in cKO and only in the central IPN
260 (**$p=0.0040$); n=4 mice per group.
261

262 Expression of $Slc17a6$ (VGLUT2) in IPN-projecting MHb neurons
263

264 The absence of $Slc17a7$/VGLUT1 expression in ChAT-expressing neurons of ventral MHb and
265 central IPN provides strong evidence for loss of VGLUT1-mediated glutamatergic co-release
266 from cholinergic MHb inputs in cKO mice. But while VGLUT1 has been implicated in mediating
267 glutamate co-release from MHb cholinergic neurons [20,35,36], there is also evidence that

268 some MHb neurons express *Slc17a6*/VGLUT2 [35,45,46], consistent with the presence of
269 VGLUT2-labeled fibers that we observed in IPN (**figure 2d**). To directly test whether *Kiaa*^{Cre}-
270 expressing MHb cells also express *Slc17a6* (VGLUT2) we used RNAscope. *Slc17a6* was
271 observed throughout the MHb (**figure 3a**), including in the ventral MHb where it partially co-
272 localized with Cre recombinase (*Kiaa*^{Cre}) (**figure 3b**).

274 The presence of MHb neurons co-expressing *Cre* and *Slc17a6* (VGLUT2) in cKO mice raised
275 the question of whether this VGLUT2 population projected to IPN. We thus injected an Adeno-
276 associated virus (AAV) into the MHb of *Slc17a6*^{Cre} (VGLUT2) mice [47] to Cre-dependently
277 express Channelrhodpsin-2 fused to a fluorescent tag (ChR2:mCherry). Three weeks after
278 surgery mCherry expression was found in MHb, as well as in surrounding areas of lateral
279 habenula (LHb) and paraventricular nucleus of the thalamus (PV) (**figure 3c**). mCherry
280 expressing fibers, presumably axon terminals from MHb, were also present in both central and
281 lateral IPN (**figure 3d**). These results indicate that at least some Kiaa^{Cre} cholinergic neurons in
282 MHb could express both VGLUT1 and VGLUT2, consistent with previous reports of
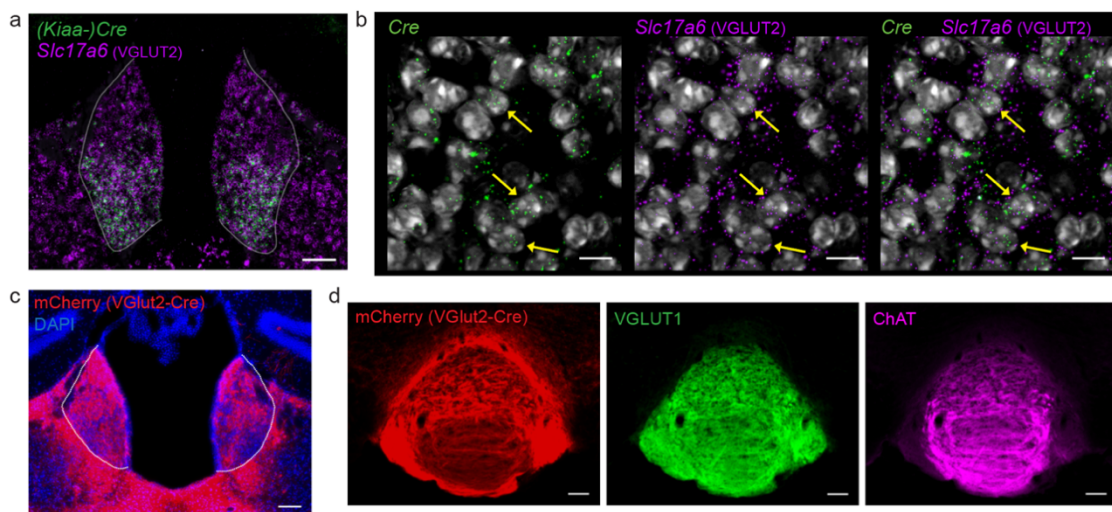283 VGLUT1/VGLUT2 co-expression in MHb [20,35].

284 **Figure 3: VGLUT2-expressing projections from MHb to IPN.**
285 **(a)** Fluorescent *in situ* hybridization from *Kiaa*^{Cre} mouse showing *Cre* and *Slc17a6* expression in
286 the MHb (outlined); scale 100 μm. **(b)** High-resolution image showing expression of *Cre*,
287 *Slc17a6* (VGLUT2), and DAPI in MHb of *Kiaa*^{Cre} mouse; scale 10 μm. Yellow arrows indicate
288 some of the cells containing both *Cre* and *Slc17a6* mRNA. **(c)** Image of MHb from *Slc17a6*^{Cre}
289 (VGLUT2) mouse injected with AAV1-Ef1α-DIO-ChR2:mCherry bilaterally into the MHb
290 (outlined); scale 100 μm. **(d)** Immunohistochemistry of IPN from *Slc17a6*^{Cre} (VGLUT2) mouse
291 injected bilaterally with AAV1-Ef1α-DIO-ChR2:mCherry in MHb. VGLUT2^{Cre} MHb terminals in
292 IPN represented by mCherry+ expression, stained with VGLUT1 and ChAT; scale 100 μm.

295 <u>Disruption of VGLUT1 from ventral MHb neurons decreased evoked glutamate currents in</u>
296 <u>central IPN</u>

298 We next tested how the loss of VGLUT1 from Cre-expressing ventral MHb cholinergic neurons
299 affected glutamate transmission from terminals in central IPN. We expressed ChR2:mCherry in
300 MHb as above, but now using *Kiaa*^{Cre} and cKO mice that lack VGLUT1 in these neurons (**figure**

8

301   **4a**). ChR2:mCherry expression was observed in MHb and IPN (**figure 4b**); recordings were
302   made from IPN neurons, with optogenetic stimulation of MHb terminals. Whole-cell voltage-
303   clamp was used to assess optogenetic evoked excitatory postsynaptic currents (oEPSC) in
304   response to either a single pulse of blue light (5ms) or train stimulation (5ms pulses at 20Hz for
305   1s). Single-pulse stimulation evoked DNQX-sensitive fast glutamatergic oEPSCs (**figure 4c**);
306   oEPSCs were significantly smaller but not eliminated in the cKO (*unpaired t-test; t(14)=4.0,*
307   *p=0.001*). Residual currents were presumably due to expression of VGLUT2 in some of the Cre-
308   expressing cholinergic neurons and were blocked by bath application of an AMPA-type
309   glutamate receptor antagonist. Train stimulation led to a mixed response that contained both
310   faster glutamatergic, as well as slower cholinergic oEPSCs (**figure 4d**) that were blocked by a
311   nicotinic acetylcholine receptor antagonist. While the variability in responses to train stimulation
312   appeared higher in the cKO, no significant difference in oEPSC amplitude was detected
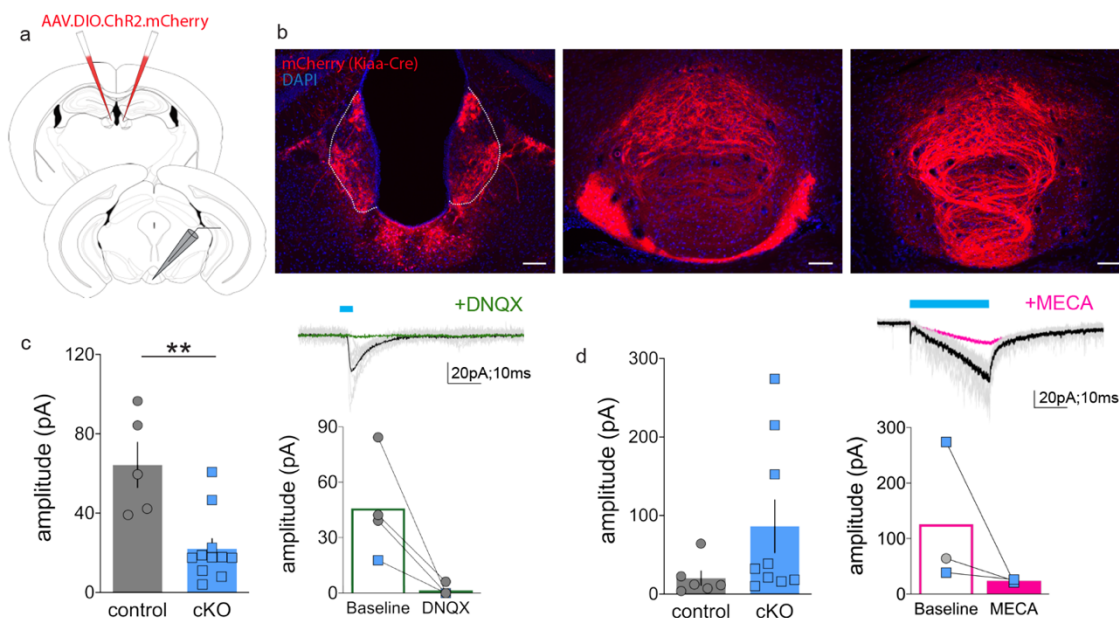313   between genotypes in response to train stimulation (*unpaired t-test; t(13)=1.6, p=0.14).*
314
315

Figure 4: Reduced glutamate transmission from MHb to IPN in VGLUT1 cKO mice.
(a) Schematic of electrophysiological preparation, with bilateral injections of AAV1-Ef1α-DIO-
ChR2:mCherry in MHb of control (*Kiaa^{Cre}*) or cKO (*Kiaa^{Cre}*; *Slc17a7$^{flox/flox}$*) mice. Slice recordings
using optogenetic stimulation performed in the IPN 3+weeks after injection. **(b)** Images from
control mouse of native Cre-dependent mCherry fluorescence in MHb (left) and fibers in IPN
(center, right); scale 100 μm. **(c)** Whole-cell recordings in IPN with single-pulse optogenetic
stimulation of MHb terminals led to oEPSC amplitudes that were reduced in the cKO (left,
p=0.001*); blocked by bath application of DNQX (right). **(d) oEPSC amplitude following train
stimulation (1s) did not differ significantly different between control and cKO groups (*left*);
sensitive to mecamylamine (right).

Loss of MHb VGLUT1 increased nicotine self-administration

329   Prior studies have implicated MHb cholinergic signaling to IPN in the aversive effects of nicotine
330   [17,18,20-22,34], but the contribution of glutamate co-release from this circuit had not been
331   examined. We thus assessed the behavioral phenotype of littermate control and cKO mice. To

332   test gross locomotor and exploratory behavior, we assessed mice in the open-field test. No
333   significant differences were found between genotype in distance traveled (*RM two-way ANOVA;*
334   *main effect of segment, F(2.6,36)=30, p<0.0001; genotype, F(1,14)=0.12, p=0.73; segment x*
335   *genotype interaction, F(5,70)=2.0, p=0.084*) (**figure 5a**) or time spent in center (*main effect of*
336   *segment, F(3.4,47)=1.1, p=0.38; genotype, F(1,14)=0.14, p=0.71; segment x genotype*
337   *interaction, F(5,70)=0.19, p=0.97*) (**figure 5b**).
338
339   Next, control and cKO mice were trained to lever press for food pellets and each reward delivery
340   was paired with a cue-light for a 20-s timeout period (TO20). Across the initial 3 sessions, the
341   fixed ratio (FR) schedule increased from 1 to 5 lever presses, then mice were maintained on an
342   FR5 for an additional 3 sessions. No significant differences between genotypes were detected,
343   suggesting intact operant learning and lever discrimination in cKO mice (*RM three-way ANOVA;*
344   *main effect of session, F(6,108)=72, p<0.0001; genotype, F(1,18)=0.10, p=0.75; lever,*
345   *F(1,18)=243, p<0.0001; session x genotype, F(6,108)=0.90, p=0.50; session x lever,*
346   *F(6,108)=74, p<0.0001; genotype x lever, F(1,18)=0.026, p=0.87; session x genotype x lever,*
347   *F(6,108)=1.3, p=0.25*) (**figure 5c**).
348
349   After food training, intravenous catheters were implanted, and an acquisition dose of nicotine
350   (0.03 mg/kg/infusion) was introduced at the established FR5 TO20 schedule of reinforcement.
351   As previously observed with this protocol [18], both groups pressed initially at a high rate similar
352   to that observed with food reinforcement, which subsequently declined across sessions to a
353   steady-state rate of nicotine self-administration (**figure 5d**). Interestingly, cKO mice engaged in
354   consistently higher levels of nicotine self-administration across sessions at this dose *(RM three-*
355   *way ANOVA; main effect of session, F(7,112)=38, p<0.0001; genotype, F(1,16)=11, p=0.004;*
356   *lever, F(1,16)=111, p<0.0001; session x genotype, F(7,112)=1.8, p=0.099; session x lever,*
357   *F(7,112)=33, p<0.0001; genotype x lever, F(1,16)=8.5, p=0.010; session x genotype x lever,*
358   *F(7,112)=0.95, p=0.47*). Compared to controls, cKO mice earned significantly more total
359   nicotine infusions in the first three test sessions *(unpaired t-test; t(16)=2.3, p=0.035)* (**figure 5e**).
360
361   To assess across a range of nicotine doses, a dose-response was then performed. While both
362   groups exhibited an inverted U-shaped dose-response, cKO mice showed a dose-dependent
363   increase in nicotine consumption compared to controls and this effect was most pronounced at
364   0.03 mg/kg/infusion dose *(RM two-way ANOVA; main effect of dose, F(4,64)=24, p<0.0001;*
365   *genotype, F(1,16)=2.4, p=0.14; dose x genotype interaction, F(4,64)=3.5, p=0.012)* (**figure 5f**).
366   Together, these results support the hypothesis that VGLUT1-mediated glutamate transmission
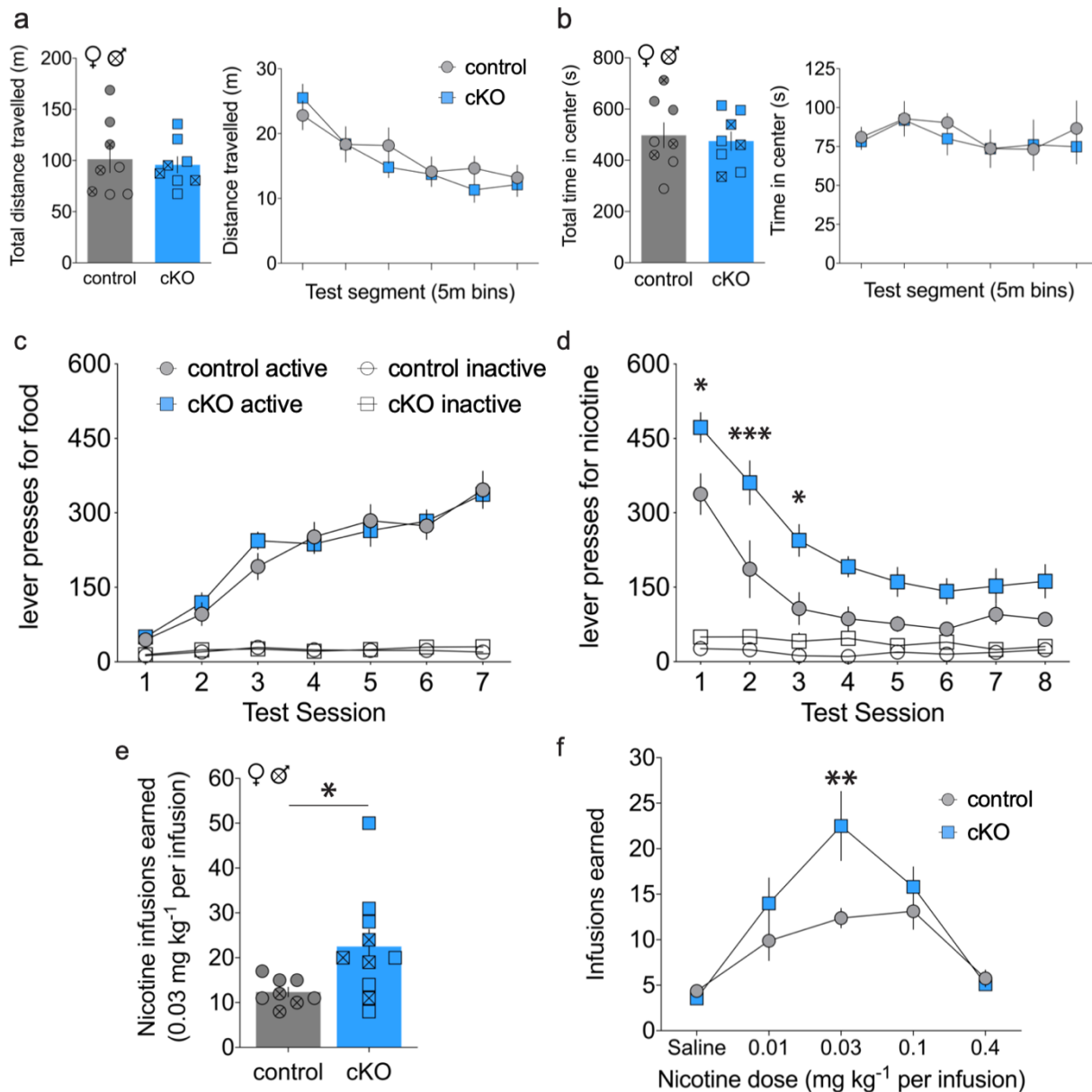367   from MHb to IPN opposes nicotine self-administration.

Figure 5: Increased nicotine self-administration in cKO mice.
(a) Total distance traveled (*left*) and distance travelled across test segments (*right*) in open field assay showed no significant differences between genotype. **(b)** Total time in center (*left*) and time in center across test segments (*right*) did not differ between genotype. **(c)** Active and inactive lever presses during food training across test session did not differ by genotype. **(d)** Active and inactive lever presses for nicotine show increased self-administration for cKO mice (*Sidak's *p<0.05, ***p<0.001).* **(e)** cKO mice earned more total nicotine infusions in first 3 nicotine test sessions (t-test, **p<0.05). (f)* Nicotine infusions earned by control and cKO mice in dose-response paradigm (*Sidak's, **p<0.01).*

DISCUSSION

Nicotine has both positively and negatively reinforcing properties. The balance of these two vary by administration route, dose, prior nicotine exposures, as well as by context, cues, schedules and contingencies [48-51]. Negative somatic and psychological effects of nicotine include nausea, dizziness, and anxiety [52,53]. Humans and monkeys will work to delay non-contingent intravenous infusions of nicotine, and higher doses can elicit conditioned place aversion in mice [54,55].

MHb projections to IPN are critical regulators of nicotine consumption. Nicotine facilitates glutamate release from MHb terminals by activating pre-synaptic α5-containing nAChRs [25,56]. Selective knock-down of α5 nAChR in MHb led to increased nicotine consumption in mice, as did blocking glutamate transmission in IPN by microinjection of NMDA-receptor antagonist [19]. More recently, targeted knock-down of α3 nAChR subunit in either MHb or IPN was shown to produce similar increases in nicotine intake [24]. Global overexpression of β4 nAChR subunit led to increased nicotine aversion, an effect reversed by selective expression of α5 nAChR subunit in MHb [21]. Together these data indicate that nicotine acting on α5-, α3-, and β4- containing nAChRs facilitates nicotine-mediated excitatory transmission at MHb synapses in the IPN, which reduces nicotine-self administration. Importantly, our data demonstrate that cKO of VGLUT1 in the MHb led to increased nicotine self-administration, which is consistent with this framework and provide the first direct evidence that release of glutamate from cholinergic MHb projections to IPN inhibits nicotine consumption.

The MHb is a heterogenous structure composed of several unique cell types, each capable of releasing or co-releasing a variety of neurotransmitters and neuropeptides [57,58]. For example, Fos data indicate that most MHb cell types are activated by foot-shock stress [57]. On the other hand, activity in dorsal MHb neurons, which are largely non-cholinergic, may play a role in positive reinforcement and reward consumption [59,60]. Further, stimulation of glutamatergic septal inputs to MHb was anxiolytic, though different populations of MHb neurons were either inhibited or excited by this manipulation [61]. Thus, different MHb cell types appear to play opposing roles in mediating behaviors and affective states relevant to nicotine consumption.

Disruption of glutamate transmission from MHb to IPN could increase nicotine self-administration if this glutamate signal opposes nicotine reward or mediates aspects of nicotine aversion, though several lines of evidence favor the latter. For example, MHb projections to the IPN mediate negative affective behaviors such as anxiety, aversion, and the expression and extinction of fear memories [19,31,61-65]. In mice undergoing nicotine withdrawal, optogenetic silencing of MHb inputs to IPN reduced marble-burying and increased time spent in the open arms of an elevated plus maze; microinjection of NMDA antagonist in IPN recapitulated this effect and was also shown to reduce somatic signs of withdrawal [66,67]. Therefore, the loss of glutamate release from cholinergic MHb projections in our study most likely led to increased nicotine consumption by reducing its aversive properties.

Previous reports have detailed activation of the central IPN by MHb projections via fast glutamate-mediated currents, as well as by slower ACh-mediated currents [20,25,36]. Histological assessments of VGLUT1 and the vesicular ACh transporter (VAChT) have shown MHb axon terminals co-positive for these transporters, and electron microscopy has identified vesicles at this synapse containing both vesicular transporters [20,35,36]. Our experiments

12

425 show presence of both *Slc17a7*/VGLUT1 and *Slc17a6*/VGLUT2 RNA transcripts in MHb, and
426 that VGLUT2-expressing MHb neurons can also project to both lateral and central IPN,
427 consistent with prior findings [57,58,68]. In our VGLUT1 cKO animals, the residual glutamate-
428 mediated oEPSCs still present in IPN are most likely facilitated by expression of VGLUT2.
429 Nevertheless, cKO of VGLUT1 led to a large reduction in evoked glutamate currents and to
430 decreased nicotine intake, though disrupting both vesicular glutamate transporters might
431 produce an even larger effect which may be addressed in future studies.
432
433 Work by Frahm and colleagues used a similar approach to disrupt ChAT expression in MHb and
434 showed that this led to loss of nicotine withdrawal behaviors and loss of nicotine conditioned
435 place preference [20]. Thus, despite both transmitters exerting primarily excitatory post-synaptic
436 actions, glutamate and ACh release from MHb neurons appear to mediate different affective
437 responses to nicotine – with cholinergic transmission necessary for nicotine-associated reward,
438 and glutamate transmission signaling nicotine aversion. This is perhaps more surprising given
439 that these transmitters localize to an overlapping pool of synaptic vesicles and synergistic
440 effects on vesicle filling are supported by data demonstrating that loss of ChAT/ACh reduces
441 glutamate filling [20], presumably because ACh uptake through VAChT dissipates the vesicular
442 pH gradient and increases the vesicular membrane potential that VGLUT relies on for
443 packaging glutamate [69]. And while we did not observe a reciprocal reduction in cholinergic
444 transmission in the VGLUT1 cKO, this may be due to high variability in detection of cholinergic
445 currents, or due to the presence of VGLUT2.
446
447 Nicotine consumption is shaped by a balance of its rewarding and aversive actions, thus our
448 understanding of the circuit mechanisms by which nicotine aversion is encoded is crucial for
449 developing effective therapeutics for nicotine addiction. Our findings demonstrate a role for
450 glutamate signals from MHb cholinergic projections to IPN in opposing nicotine self-
451 administration and suggests that potentiating nicotine's effect on this circuit could be a useful
452 target for nicotine cessation therapies. Future work may also focus on dissecting the relative
453 roles of glutamate, ACh or other co-transmitters in this circuit on other aspects of nicotine
454 behavior or in mediating responses to other substances of abuse.
455
456

462
463 **AUTHOR CONTRIBUTIONS**
464 TSH conceived of the project. EAS, YC, VZ, YL, TS, WSC, WW, KDH, CDF and TSH
465 contributed to data acquisition and analysis. EAS, WSC, CDF and TSH wrote the manuscript
466 with input by all authors.

REFERENCES

1 Wang TW, Gentzke AS, Creamer MR, Cullen KA, Holder-Hayes E, Sawdey MD, et al. Tobacco Product Use and Associated Factors Among Middle and High School Students — United States, 2019. MMWR Surveillance Summaries. 2019;68(12):1-22.

2 Kasza KA, Ambrose BK, Conway KP, Borek N, Taylor K, Goniewicz ML, et al. Tobacco-Product Use by Adults and Youths in the United States in 2013 and 2014. New England Journal of Medicine. 2017;376(4):342-53.

3 Cooper SY, Henderson BJ. The Impact of Electronic Nicotine Delivery System (ENDS) Flavors on Nicotinic Acetylcholine Receptors and Nicotine Addiction-Related Behaviors. Molecules. 2020;25(18):4223.

4 Dani JA, Heinemann S. Molecular and Cellular Aspects of Nicotine Abuse. Neuron. 1996;16(5):905-08.

5 Mansvelder HD, McGehee DS. Cellular and synaptic mechanisms of nicotine addiction. Journal of Neurobiology. 2002;53(4):606-17.

6 Wittenberg RE, Wolfman SL, De Biasi M, Dani JA. Nicotinic acetylcholine receptors and nicotine addiction: A brief introduction. Neuropharmacology. 2020;177:108256.

7 Akers AT, Cooper SY, Baumgard ZJ, Casinelli GP, Avelar AJ, Henderson BJ. Upregulation of nAChRs and Changes in Excitability on VTA Dopamine and GABA Neurons Correlates to Changes in Nicotine-Reward-Related Behavior. eNeuro. 2020;7(5):ENEURO.0189-20.

8 Calabresi P, Lacey MG, North RA. Nicotinic excitation of rat ventral tegmental neurones in vitro studied by intracellular recording. British Journal of Pharmacology. 1989;98(1):135-40.

9 Grieder TE, Besson M, Maal-Bared G, Pons S, Maskos U, Van Der Kooy D. β2* nAChRs on VTA dopamine and GABA neurons separately mediate nicotine aversion and reward. Proceedings of the National Academy of Sciences. 2019;116(51):25968-73.

10 Liu L, Zhao-Shea R, Mcintosh JM, Gardner PD, Tapper AR. Nicotine Persistently Activates Ventral Tegmental Area Dopaminergic Neurons via Nicotinic Acetylcholine Receptors Containing α4 and α6 Subunits. Molecular Pharmacology. 2012;81(4):541-48.

11 Mansvelder HD, McGehee DS. Long-Term Potentiation of Excitatory Inputs to Brain Reward Areas by Nicotine. Neuron. 2000;27(2):349-57.

12 Peng C, Engle SE, Yan Y, Weera MM, Berry JN, Arvin MC, et al. Altered nicotine reward-associated behavior following α4 nAChR subunit deletion in ventral midbrain. PLOS ONE. 2017;12(7):e0182142.

13 Pons S, Fattore L, Cossu G, Tolu S, Porcu E, Mcintosh JM, et al. Crucial Role of α4 and α6 Nicotinic Acetylcholine Receptor Subunits from Ventral Tegmental Area in Systemic Nicotine Self-Administration. Journal of Neuroscience. 2008;28(47):12318-27.

504   14   Pontieri FE, Tanda G, Orzi F, Chiara GD. Effects of nicotine on the nucleus accumbens
505   and similarity to those of addictive drugs. Nature. 1996;382(6588):255-57.

506   15   Antolin-Fontes B, Ables JL, Görlich A, Ibañez-Tallon I. The habenulo-interpeduncular
507   pathway in nicotine aversion and withdrawal. Neuropharmacology. 2015;96(Pt B):213-
508   22.

509   16   Antolin-Fontes B, Li K, Ables JL, Riad MH, Görlich A, Williams M, et al. The habenular
510   G-protein–coupled receptor 151 regulates synaptic plasticity and nicotine intake.
511   Proceedings of the National Academy of Sciences of the United States of America.
512   2020;117(10):5502-09.

513   17   Fowler CD, Kenny PJ. Nicotine aversion: Neurobiological mechanisms and relevance to
514   tobacco dependence vulnerability. Neuropharmacology. 2014;76:533-44.

515   18   Fowler CD, Kenny PJ. Intravenous nicotine self-administration and cue-induced
516   reinstatement in mice: Effects of nicotine dose, rate of drug infusion and prior
517   instrumental training. Neuropharmacology. 2011;61(4):687-98.

518   19   Fowler CD, Lu Q, Johnson PM, Marks MJ, Kenny PJ. Habenular α5 nicotinic receptor
519   subunit signalling controls nicotine intake. Nature. 2011;471(7340):597–601.

520   20   Frahm S, Antolin-Fontes B, Görlich A, Zander JF, Ahnert-Hilger G, Ibañez-Tallon I. An
521   essential role of acetylcholine- glutamate synergy at habenular synapses in nicotine
522   dependence. eLife. 2015;4:e11396.

523   21   Frahm S, Ślimak MA, Ferrarese L, Santos-Torres J, Antolin-Fontes B, Auer S, et al.
524   Aversion to Nicotine Is Regulated by the Balanced Activity of β4 and α5 Nicotinic
525   Receptor Subunits in the Medial Habenula. Neuron. 2011;70(3):522-35.

526   22   Salas R, Sturm R, Boulter J, De Biasi M. Nicotinic receptors in the habenulo-
527   interpeduncular system are necessary for nicotine withdrawal in mice. Journal of
528   Neuroscience. 2009;29(10):3014-18.

529   23   Tuesta LM, Chen Z, Duncan A, Fowler CD, Ishikawa M, Lee BR, et al. GLP-1 acts on
530   habenular avoidance circuits to control nicotine intake. Nature Neuroscience.
531   2017;20(5):708-16.

532   24   Elayouby KS, Ishikawa M, Dukes AJ, Smith ACW, Lu Q, Fowler CD, et al. α3* Nicotinic
533   Acetylcholine Receptors in the Habenula-Interpeduncular Nucleus Circuit Regulate
534   Nicotine Intake. The Journal of Neuroscience. 2021;41(8):1779-87.

535   25   McGehee DS, Heath MJS, Gelber S, Devay P, Role LW. Nicotine enhancement of fast
536   excitatory synaptic transmission in CNS by presynaptic receptors. Science.
537   1995;269(5231):1692-96.

538   26   Perry DC, Xiao Y, Nguyen HN, Musachio JL, Dávila-Garcí MI, Kellar KJ. Measuring
539   nicotinic receptors with characteristics of α4β2, α3β2 and α3β4 subtypes in rat tissues by
540   autoradiography. Journal of Neurochemistry. 2002;82(3):468-81.

541   27   Salas R, Pieri F, De Biasi M. Decreased signs of nicotine withdrawal in mice null for the
542   β4 nicotinic acetylcholine receptor subunit. Journal of Neuroscience. 2004;24(45):10035-
543   39.

544   28   Shih PY, Engle SE, Oh G, Deshpande P, Puskar NL, Lester HA, et al. Differential
545   Expression and Function of Nicotinic Acetylcholine Receptors in Subdivisions of Medial
546   Habenula. Journal of Neuroscience. 2014;34(29):9789-802.

547   29   Dineley-Miller K, Patrick J. Gene transcripts for the nicotinic acetylcholine receptor
548   subunit, beta4, are distributed in multiple areas of the rat central nervous system.
549   Molecular Brain Research. 1992;16(3-4):339-44.

550   30   Marks M, Pauly J, Gross S, Deneris E, Hermans-Borgmeyer I, Heinemann S, et al.
551   Nicotine binding and nicotinic receptor subunit RNA after chronic nicotine treatment. The
552   Journal of Neuroscience. 1992;12(7):2765-84.

553   31   Wolfman SL, Gill DF, Bogdanic F, Long K, Al-Hasani R, McCall JG, et al. Nicotine
554   aversion is mediated by GABAergic interpeduncular nucleus inputs to laterodorsal
555   tegmentum. Nature Communications. 2018;9(1):2710.

556   32   Contestabile A, Villani L, Fasolo A, Franzoni MF, Gribaudo L, Øktedalen O, et al.
557   Topography of cholinergic and substance P pathways in the habenulo-interpeduncular
558   system of the rat. An immunocytochemical and microchemical approach. Neuroscience.
559   1987;21(1):253-70.

560   33   Herkenham M, Nauta WJH. Efferent connections of the habenular nuclei in the rat.
561   Journal of Comparative Neurology. 1979;187(1):19-47.

562   34   Harrington L, Viñals X, Herrera-Solís A, Flores A, Morel C, Tolu S, et al. Role of β4∗
563   Nicotinic Acetylcholine Receptors in the Habenulo-Interpeduncular Pathway in Nicotine
564   Reinforcement in Mice. Neuropsychopharmacology. 2016;41(7):1790-802.

565   35   Aizawa H, Kobayashi M, Tanaka S, Fukai T, Okamoto H. Molecular characterization of
566   the subnuclei in rat habenula. The Journal of Comparative Neurology.
567   2012;520(18):4051-66.

568   36   Ren J, Qin C, Hu F, Tan J, Qiu L, Zhao S, et al. Habenula "Cholinergic" Neurons
569   Corelease Glutamate and Acetylcholine and Activate Postsynaptic Neurons via Distinct
570   Transmission Modes. Neuron. 2011;69(3).

571   37   Faget L, Zell V, Souter E, McPherson A, Ressler R, Gutierrez-Reed N, et al. Opponent
572   control of behavioral reinforcement by inhibitory and excitatory projections from the
573   ventral pallidum. Nature Communications. 2018;9(1).

574   38   Chen E, Lallai V, Sherafat Y, Grimes NP, Pushkin AN, Fowler J, et al. Altered Baseline
575   and Nicotine-Mediated Behavioral and Cholinergic Profiles in ChAT-Cre Mouse Lines.
576   The Journal of Neuroscience. 2018;38(9):2177-88.

577   39   Zell V, Steinkellner T, Hollon NG, Warlow SM, Souter E, Faget L, et al. VTA Glutamate
578   Neuron Activity Drives Positive Reinforcement Absent Dopamine Co-release. Neuron.
579   2020;107(5):864-73.

40 Madisen L, Zwingman TA, Sunkin SM, Oh SW, Zariwala HA, Gu H, et al. A robust and high-throughput Cre reporting and characterization system for the whole mouse brain. Nature Neuroscience. 2010;13(1):133-40.

41 Görlich A, Antolin-Fontes B, Ables JL, Frahm S, Ślimak MA, Dougherty JD, et al. Reexposure to nicotine during withdrawal increases the pacemaking activity of cholinergic habenular neurons. Proceedings of the National Academy of Sciences of the United States of America. 2013;110(42):17077-82.

42 Oh JD, Woolf NJ, Roghani A, Edwards RH, Butcher LL. Cholinergic neurons in the rat central nervous system demonstrated by in situ hybridization of choline acetyltransferase mRNA. Neuroscience. 1992;47(4):807-22.

43 Trifonov S, Houtani T, Hamada S, Kase M, Maruyama M, Sugimoto T. In situ hybridization study of the distribution of choline acetyltransferase mRNA and its splice variants in the mouse brain and spinal cord. Neuroscience. 2009;159(1):344-57.

44 Fremeau RT, Troyer MD, Pahner I, Nygaard GO, Tran CH, Reimer RJ, et al. The expression of vesicular glutamate transporters defines two classes of excitatory synapse. Neuron. 2001;31(2):247-60.

45 Barroso-Chinea P, Castle M, Aymerich MS, Pérez-Manso M, Erro E, Tuñon T, et al. Expression of the mRNAs encoding for the vesicular glutamate transporters 1 and 2 in the rat thalamus. Journal of Comparative Neurology. 2007;501(5):703-15.

46 Varoqui H, Schäfer MKH, Zhu H, Weihe E, Erickson JD. Identification of the differentiation-associated Na+/PI transporter as a novel vesicular glutamate transporter expressed in a distinct set of glutamatergic synapses. Journal of Neuroscience. 2002;22(1):142-55.

47 Vong L, Ye C, Yang Z, Choi B, Chua S, Lowell BB. Leptin Action on GABAergic Neurons Prevents Obesity and Reduces Inhibitory Tone to POMC Neurons. Neuron. 2011;71(1):142-54.

48 Sartor CE, Lessov-Schlaggar CN, Scherrer JF, Bucholz KK, Madden PA, Pergadia ML, et al. Initial response to cigarettes predicts rate of progression to regular smoking: findings from an offspring-of-twins design. Addict Behav. 2010;35(8):771-8.

49 Dong Y, Zhang T, Li W, Doyon WM, Dani JA. Route of nicotine administration influences in vivo dopamine neuron activity: habituation, needle injection, and cannula infusion. J Mol Neurosci. 2010;40(1-2):164-71.

50 Corrigall WA, Coen KM. Nicotine maintains robust self-administration in rats on a limited-access schedule. Psychopharmacology (Berl). 1989;99(4):473-8.

51 Henningfield JE, Goldberg SR. Nicotine as a reinforcer in human subjects and laboratory animals. Pharmacol Biochem Behav. 1983;19(6):989-92.

52 Zevin S, Gourlay SG, Benowitz NL. Clinical pharmacology of nicotine. Clin Dermatol. 1998;16(5):557-64.

618   53   File SE, Cheeta S, Kenny PJ. Neurobiological mechanisms by which nicotine mediates
619   different types of anxiety. Eur J Pharmacol. 2000;393(1-3):231-6.

620   54   Spealman RD. Maintenance of behavior by postponement of scheduled injections of
621   nicotine in squirrel monkeys. J Pharmacol Exp Ther. 1983;227(1):154-9.

622   55   Risinger FO, Oakes RA. Nicotine-induced conditioned place preference and conditioned
623   place aversion in mice. Pharmacol Biochem Behav. 1995;51(2-3):457-61.

624   56   Girod R, Barazangi N, Mcgehee D, Role LW. Facilitation of glutamatergic
625   neurotransmission by presynaptic nicotinic acetylcholine receptors. Neuropharmacology.
626   2000;39(13):2715-25.

627   57   Hashikawa Y, Hashikawa K, Rossi MA, Basiri ML, Liu Y, Johnston NL, et al.
628   Transcriptional and Spatial Resolution of Cell Types in the Mammalian Habenula.
629   Neuron. 2020;106(5):743-58.e5.

630   58   Wallace ML, Huang KW, Hochbaum D, Hyun M, Radeljic G, Sabatini BL. Anatomical
631   and single-cell transcriptional profiling of the murine habenular complex. Elife. 2020;9.

632   59   Hsu YW, Wang SD, Wang S, Morton G, Zariwala HA, de la Iglesia HO, et al. Role of the
633   dorsal medial habenula in the regulation of voluntary activity, motor function, hedonic
634   state, and primary reinforcement. J Neurosci. 2014;34(34):11366-84.

635   60   Hsu YW, Morton G, Guy EG, Wang SD, Turner EE. Dorsal Medial Habenula Regulation
636   of Mood-Related Behaviors and Primary Reinforcement by Tachykinin-Expressing
637   Habenula Neurons. eNeuro. 2016;3(3).

638   61   Otsu Y, Darcq E, Pietrajtis K, Matyas F, Schwartz E, Bessaih T, et al. Control of aversion
639   by glycine-gated GluN1/GluN3A NMDA receptors in the adult medial habenula. Science.
640   2019;366(6462):250-54.

641   62   Pang X, Liu L, Ngolab J, Zhao-Shea R, McIntosh JM, Gardner PD, et al. Habenula
642   cholinergic neurons regulate anxiety during nicotine withdrawal via nicotinic
643   acetylcholine receptors. Neuropharmacology. 2016;107:294-304.

644   63   Soria-Gomez E, Busquets-Garcia A, Hu F, Mehidi A, Cannich A, Roux L, et al.
645   Habenular CB1 Receptors Control the Expression of Aversive Memories. Neuron.
646   2015;88(2):306-13.

647   64   Yamaguchi R, Nicholson Perry K, Hines M. Pain, pain anxiety and emotional and
648   behavioural problems in children with cerebral palsy. Disabil Rehabil. 2014;36(2):125-30.

649   65   Zhang J, Tan L, Ren Y, Liang J, Lin R, Feng Q, et al. Presynaptic Excitation via GABAB
650   Receptors in Habenula Cholinergic Neurons Regulates Fear Memory Expression. Cell.
651   2016;166(3):716-28.

652   66   Zhao-Shea R, Liu L, Pang X, Gardner PD, Tapper AR. Activation of GABAergic neurons
653   in the interpeduncular nucleus triggers physical nicotine withdrawal symptoms. Current
654   Biology. 2013;23(23):2327-35.

655   67   Zhao-Shea R, DeGroot SR, Liu L, Vallaster M, Pang X, Su Q, et al. Increased CRF
656   signalling in a ventral tegmental area-interpeduncular nucleus-medial habenula circuit
657   induces anxiety during nicotine withdrawal. Nat Commun. 2015;6:6770.

658   68   Qin C, Luo M. Neurochemical phenotypes of the afferent and efferent projections of the
659   mouse medial habenula. Neuroscience. 2009;161(3):827-37.

660   69   Hnasko TS, Edwards RH. Neurotransmitter corelease: mechanism and physiological
661   role. Annu Rev Physiol. 2012;74:225-43.
662